Placental trophoblast syncytialization potentiates macropinocytosis via mTOR signaling to adapt to reduced amino acid supply

Xuan Shao[a,b,c,1], Guangming Cao[d,1], Dunjin Chen[e,1], Juan Liu[a,c], Bolan Yu[e], Ming Liu[a], Yu-Xia Li[a], Bin Cao[f,2], Yoel Sadovsky[g,h,2], and Yan-Ling Wang[a,b,c,2]

[a]State Key Laboratory of Stem Cell and Reproductive Biology, Institute of Zoology, Chinese Academy of Sciences, 100101 Beijing, China; [b]Stem Cell and Regenerative Medicine Innovation Institute, Chinese Academy of Sciences, 100101 Beijing, China; [c]University of Chinese Academy of Sciences, 101408 Beijing, China; [d]Department of Obstetrics and Gynecology, Beijing Chao-Yang Hospital, Capital Medical University, 100020 Beijing, China; [e]Department of Obstetrics and Gynecology, The Third Affiliated Hospital of Guangzhou Medical University, 510150 Guangzhou, China; [f]Fujian Provincial Key Laboratory of Reproductive Health Research, School of Medicine, Xiamen University, 361102 Xiamen, China; [g]Department of Obstetrics, Gynecology, and Reproductive Sciences, Magee-Womens Research Institute, University of Pittsburgh, Pittsburgh, PA 15213; and [h]Department of Microbiology and Molecular Genetics, University of Pittsburgh, Pittsburgh, PA 15219

Edited by R. Michael Roberts, University of Missouri, Columbia, MO, and approved December 7, 2020 (received for review August 13, 2020)

During pregnancy, the appropriate allocation of nutrients between the mother and the fetus is dominated by maternal–fetal interactions, which is primarily governed by the placenta. The syncytiotrophoblast (STB) lining at the outer surface of the placental villi is directly bathed in maternal blood and controls feto–maternal exchange. The STB is the largest multinucleated cell type in the human body, and is formed through syncytialization of the mononucleated cytotrophoblast. However, the physiological advantage of forming such an extensively multinucleated cellular structure remains poorly understood. Here, we discover that the STB uniquely adapts to nutrient stress by inducing the macropinocytosis machinery through repression of mammalian target of rapamycin (mTOR) signaling. In primary human trophoblasts and in trophoblast cell lines, differentiation toward a syncytium triggers macropinocytosis, which is greatly enhanced during amino acid shortage, induced by inhibiting mTOR signaling. Moreover, inhibiting mTOR in pregnant mice markedly stimulates macropinocytosis in the syncytium. Blocking macropinocytosis worsens the phenotypes of fetal growth restriction caused by mTOR-inhibition. Consistently, placentas derived from fetal growth restriction patients display: 1) Repressed mTOR signaling, 2) increased syncytialization, and 3) enhanced macropinocytosis. Together, our findings suggest that the unique ability of STB to undergo macropinocytosis serves as an essential adaptation to the cellular nutrient status, and support fetal survival and growth under nutrient deprivation.

placental syncytiotrophoblast | macropinocytosis | mTOR | amino acid shortage | fetal growth

During pregnancy, the health of the mother and the fetus is dominated by the appropriate allocation of nutrients between the two individuals. Maternal–fetal material exchange predominantly depends on the placenta, which is responsible for transferring the bulk of nutrients between maternal and fetal circulations. The placenta plays a critical role in sensing fetal nutritional demands, modulating maternal supply, and adapting its nutrient transport capacity. Limited maternal nutrient availability can lead to adaptive changes in the placental endocrine function, which is thought to attenuate the potential conflict between fetal growth demands and maternal health (1).

Fetal growth restriction (FGR) represents a pregnancy complication whereby the fetus fails to attain its genetically determined growth potential due to insufficient delivery of maternal nutrition, especially amino acids, by the placenta (1–3). Annually, ∼30 million newborns, mainly in developing countries, suffer from FGR (4), which leads to increased perinatal morbidity and mortality and multiple lifelong health problems (5). The mechanisms deployed by the placenta to compensate nutrient-deprivation injury and support fetal survival remain unknown.

At the outermost surface of the placenta, the syncytial layer lines the placental villi, with a continuous surface measuring 12 to 14 m^2 at term (6). This layer is directly bathed in maternal blood, and thus positioned to regulate feto–maternal exchanges of gases, nutrients, and waste. The syncytial layer comprises the multinucleated syncytiotrophoblast (STB), the largest multinucleated epithelial surface in the body, which is formed through fusion of the mononucleated cytotrophoblast (CTB). Yet, the physiological advantages of forming such an extensive multinucleated cellular structure and the regulatory mechanisms underlying this process remain to be explored.

Macropinocytosis constitutes a specialized route for cellular nutrient uptake from the fluid phase. It is functional in certain cell types, including immature dendritic cells, macrophages, podocytes, and tumor cells (7–10). The process involves the formation of large vesicles of 0.2 to 5 μm in diameter at the sites of membrane ruffling (11). Macropinocytosis promotes the uptake of fluid phase-derived molecules by at least 10-fold (12), especially

Significance

The appropriate allocation of nutrients between the mother and the fetus during pregnancy is predominantly governed by the syncytiotrophoblast lining at the outer surface of the placental villi. To date the advantages of such an extensively multinucleated cellular structure in substance exchange remains poorly understood. In this study, we discovered that differentiation of trophoblasts toward syncytium triggers an endocytosis strategy, macropinocytosis, to uptake large extracellular molecules. The unique uptake machinery is strikingly boosted via inhibition of mammalian target of rapamycin signaling under amino acid shortage conditions, which is essential for fetal survival. The findings highlight an adaptive mechanism of syncytiotrophoblast that senses nutrient status and support fetal survival under nutrient deprivation.

Author contributions: X.S., Y.S., and Y.-L.W. designed research; X.S., G.C., D.C., J.L., and M.L. performed research; B.Y. and Y.-X.L. contributed new reagents/analytic tools; X.S., G.C., D.C., J.L., M.L., B.C., Y.S., and Y.-L.W. analyzed data; and X.S., B.C., Y.S., and Y.-L.W. wrote the paper.

The authors declare no competing interest.

This article is a PNAS Direct Submission.

[1]X.S., G.C., and D.C. contributed equally to this work.

[2]To whom correspondence may be addressed. Email: caobin19@xmu.edu.cn, ysadovsky@mwri.magee.edu, or wangyl@ioz.ac.cn.

This article contains supporting information online at https://www.pnas.org/lookup/suppl/doi:10.1073/pnas.2017092118/-/DCSupplemental.

Published January 5, 2021.

with respect to internalization of large-sized molecules (>70 kDa) (7). In tumor cells, deprivation of amino acid supply inhibits mammalian target of rapamycin (mTOR) and enhances macropinocytosis and lysosomal catabolism of extracellular proteins to sustain cell survival and growth (13, 14), indicating macropinocytosis as an efficient way to attenuate nutrient shortage in the high-demanding cells.

Based on the above evidence, we hypothesized that trophoblasts, particularly STB, may utilize macropinocytosis to facilitate nutrient absorption from the maternal environment, thereby negotiating fetal demands in the face of diminished maternal supply. We tested our hypothesis by using cultures of primary human trophoblast (PHT) cells, human trophoblast cell lines, and rapamycin-treated pregnant mice, and demonstrated the physiological significance of macropinocytosis in STB to adapt to maternal undernutrition stress during pregnancy.

Results

Macropinocytosis Accompanies Syncytialization in Human Trophoblast. Macropinocytosis has been characterized as a metabolic rewiring and adaptation strategy to meet the high energy demands and sustain rapid cell proliferation in a nutrient-depleted microenvironment (13). We reasoned that the trophoblast, especially the STB, could undergo macropinocytosis to keep energy homeostasis and support fast fetal growth in the uterus. First, we performed in vitro trophoblast syncytialization experiments by using two cell models, spontaneously formed STB from PHT cells or forskolin (FSK)-induced cell fusion in the trophoblast cell line BeWo (15). PHT cells, isolated from normal term placenta, fused spontaneously to form STB in 10% FBS-supplemented culture condition, as indicated by a gradually increased expression of Syncytin2 (Fig. 1 *A* and *B*) and *hCGB* (the gene encoding hCGβ) (Fig. 1*C*), the hallmarks of trophoblast syncytialization (15). STB formation proceeded over time as presented by immunostaining for E-cadherin and DAPI (Fig. 1 *D* and *E*).

Next, we examined the extent of macropinocytosis using a "macropinocytic index" that monitors the incorporation of the fluorescence-labeled high molecular mass dextran (>70 KDa) from the culture medium into the intracellular space. Due to dextran's large molecular weight, it can be specifically internalized from the liquid phase via macropinocytosis (7, 14). Using confocal imaging to detect intracellular fluorescent puncta at 30 min after incubation with >70 kDa FITC-dextran, we found that dextran signal was rarely observed in PHT cells before 12 h in culture, yet intracellular FITC intensity increased substantially at 24 to 72 h (Fig. 1 *F* and *G*), pointing to enhanced macropinocytosis during syncytialization of PHT cells. Consistently, we inhibited the PHT cell fusion by adding 1.5% dimethyl sulfoxide (DMSO) (16), which repressed the expression of Syncytin2 and hCGβ, and observed diminished intracellular FITC intensity along with attenuation of syncytium formation (*SI Appendix*, Fig. S1 *A–F*).

Furthermore, we induced the time-dependent differentiation of BeWo cells into multinucleated syncytial cells by using FSK, a PKA agonist, as shown by elevated expression of STB markers Syncytin2 and *hCGB* (Fig. 1 *H–J*), and the corresponding changes of cellular morphology (Fig. 1 *K* and *L*). Importantly, similar to our findings in PHT cells, we found that macropinocytosis in FSK-exposed BeWo cells paralleled syncytialization, with increased uptake of FITC-dextran at 12 h of FSK exposure, and gradually enhanced to threefold of control at 72 h (Fig. 1 *M* and *N*). Therefore, syncytialization induced by FSK correlated with enhanced macropinocytosis in BeWo cells. To exclude the possibility that the enhanced macropinocytosis in BeWo cells was caused by FSK but independent of syncytialization, we performed identical experiments in the JEG-3 and HTR8/SVneo trophoblastic cell lines, which exhibit a very low level of syncytialization upon FSK treatment (17). FSK exposure in these cells had no effect on macropinocytosis (*SI Appendix*, Fig. S1 *G*, *H*, *J*, and *K*). We were also unable to detect macropinocytosis upon exposure of FSK in HepG2 cells, a hepatocellular carcinoma cell line (*SI Appendix*, Fig. S1 *I* and *L*). Together, these results demonstrate that the formation of human STB is associated with enhanced macropinocytosis and suggest that macropinocytosis occurs specifically in trophoblasts committed to differentiate toward the syncytium.

Reduced Supply of Amino Acids Promoted Trophoblast Syncytialization and Macropinocytosis. Given that the availability of amino acids directly correlated with the level of macropinocytosis (14, 18), we reasoned that amino acid shortage (AAS) could signal nutrient deprivation and promote adaptive trophoblast syncytialization and macropinocytosis. To mimic a restricted nutrient stress to the placenta, we cultured BeWo cells for 48 h in a well-established generic AAS medium (19, 20), in which the concentration of three amino acids (glutamine [Glu], lysine [Lys], and arginine [Arg]) were one-eighth of normal levels. Exposure to AAS increased the baseline level of hCGβ to 1.2-fold, and enhanced FSK-induced expressions of hCGβ and Syncytin2 by 94% and 50%, respectively (Fig. 2 *A–C*). Importantly, AAS promoted cell fusion and macropinocytosis, and further potentiated FSK-stimulated syncytialization and macropinocytosis in BeWo cells (Fig. 2 *D–F*). To verify the effect of AAS on macropinocytosis, we also exposed PHT cells in AAS medium. We found that hCGβ and Syncytin2 expression, syncytium formation index, and FITC-dextran incorporation demonstrated enhanced cell syncytialization and macropinocytosis in PHT cells (*SI Appendix*, Fig. S2 *A–C* and *E–G*). However, when the spontaneous syncytialization of PHT cells were blocked by 1.5% DMSO, the effect of AAS on cell fusion and dextran uptake was diminished (*SI Appendix*, Fig. S2 *A–C* and *E–G*). Together, these data indicate that amino acid deprivation leads to enhanced syncytialization and macropinocytosis in placental trophoblasts.

Attenuation of mTOR Signaling Is Necessary for AAS-Induced Macropinocytosis in Syncytialized Trophoblasts. Given that mTOR signal is a sensor and central regulator of nutrient availability and metabolism, we hypothesized that AAS-induced trophoblast syncytialization and macropinocytosis were dependent on mTOR activity. Activated AMP-activated protein kinase (AMPK) is known to repress mTOR (21), and mTOR activation further phosphorylates multiple targets, such as S6 kinase (S6K) and eukaryotic initiation factor 4E-binding protein (4E-BP) (22). In BeWo cells, the enhanced syncytialization and macropinocytosis induced by AAS alone or in combination with FSK was accompanied by the activation of AMPK and inhibition of mTOR signaling, as shown by the expression of p-AMPK/AMPK, p-S6K/S6K, and mTOR protein (Fig. 2 *G–J*). In PHT cells, deprivation of amino acids led to a lower level of p-S6K/S6K as well (*SI Appendix*, Fig. S2 *A* and *D*). Thus, the processes of syncytialization and macropinocytosis in human trophoblasts are inversely correlated with mTOR signaling.

To test whether blocking mTOR is sufficient to recapitulate the effect of AAS medium, BeWo cells were exposed to rapamycin (Rapa) or Torin, the specific short-term inhibitors of mTOR. We observed a marked repression of basal or FSK-induced mTOR activation, as validated by the reduced p-S6K/S6K (Fig. 3 *A* and *B* and *SI Appendix*, Fig. S3 *A* and *B*). In these cells, FSK-induced hCGβ and Syncytin2 expression, as well as syncytium formation, were enhanced by Rapa and Torin (Fig. 3 *A*, *C*, and *D* and *SI Appendix*, Fig. S3 *A*, *C*, and *D*). In parallel, Rapa and Torin boosted basal or FSK-stimulated cellular uptake of FITC-dextran (Fig. 3 *E–G* and *SI Appendix*, Fig. S3 *E* and *F*). Consistently, small-interfering RNA (siRNA)-mediated knockdown of Raptor, the essential component of mTORC1, in BeWo cells resulted in repression of p-S6K/S6K and enhancement of syncytialization and macropinocytosis (*SI Appendix*, Fig. S3 *G–M*). In PHT cells, blocking mTOR activation by Rapa also sufficiently recapitulated

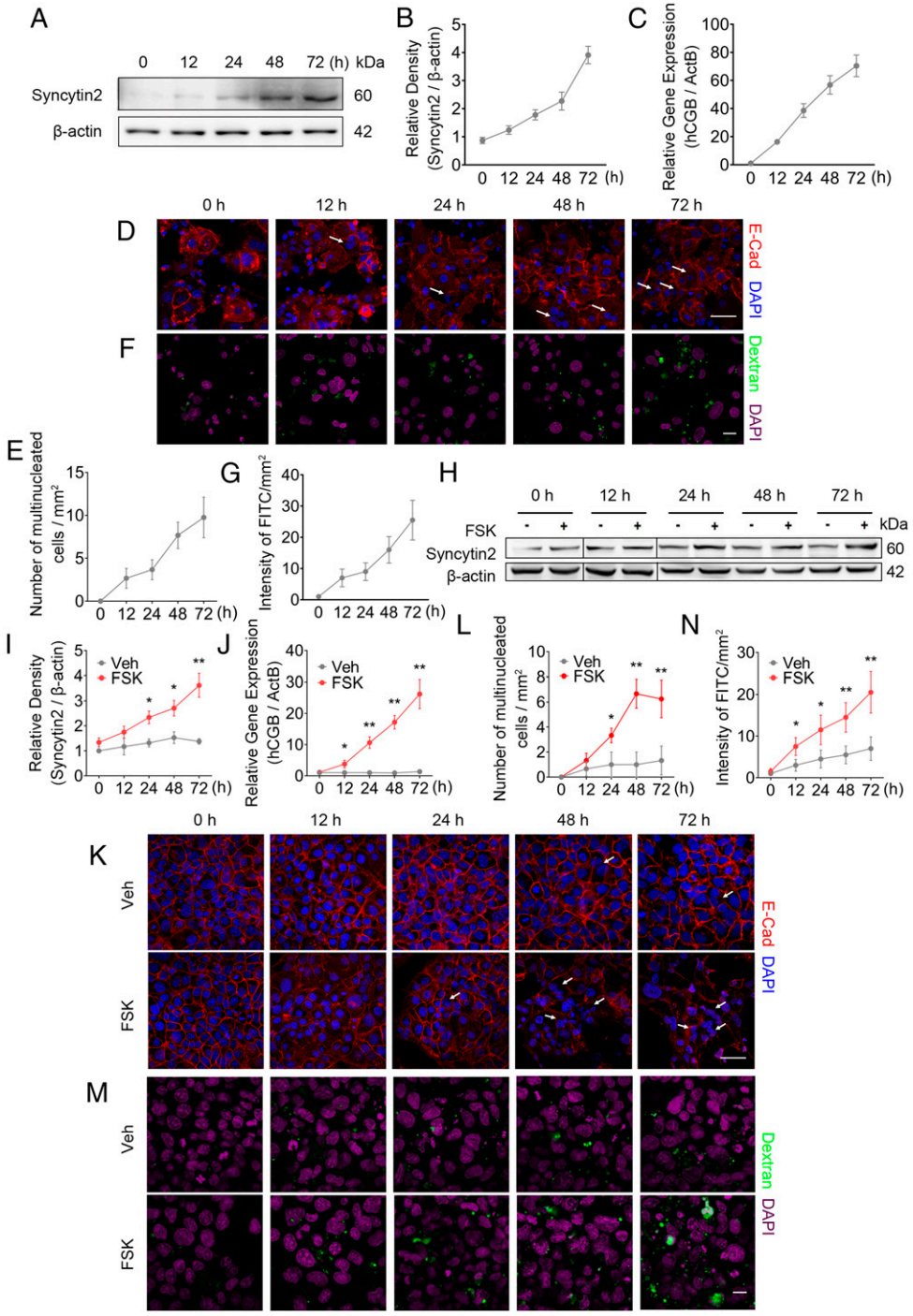

Fig. 1. Syncytialization is associated with higher levels of macropinocytosis in human trophoblasts. (*A*–*C*) Western blot of Syncytin2 (*A* and *B*) and mRNA level of *hCGB* (*C*) in term PHT cells. (*D* and *E*) Immunostainings of E-cadherin (red) and DAPI (blue) in primary CTBs from normal term placenta, showing spontaneous syncytialization. (*D*) Representative image of syncytialized trophoblasts. White arrows, multinucleated trophoblasts. (Scale bar, 40 μm.) (*E*) Quantification of multinucleated cell. E-cadherin staining outlines cell boundary. The number of multinucleated cells was calculated by counting total number of cells with at least two nuclei in five randomly selected fields per sample, three replicates per group. The results are presented as mean ± SD per square millimeter per group. (*F* and *G*) Representative FITC-dextran uptake, reflecting macropinocytosis in primary trophoblasts. (*F*) Representative confocal images showing the intracellular accumulation of fluorescent puncta after 30-min incubation in medium that was supplemented by >70 kDa FITC-dextran. Green and magenta signals indicate FITC-dextran and DAPI, respectively. The macropinocytosis activity was analyzed using ImageJ software (NIH). The "Smooth" feature in ImageJ was employed after background subtraction and before threshold adjustments. The area of FITC-labeled macropinosomes was determined using the "Analyze Particles" feature in ImageJ, and the intensity of FITC of macropinosomes was computed by the mean area of five randomly selected fields per slide, three slides per group (47). (Scale bar, 40 μm.) (*G*) A time course of FITC intensity reflecting macropinocytosis in trophoblasts. (*H*–*J*) Western blot of Syncytin2 (*H* and *I*) and mRNA (RT-qPCR) of *hCGB* (*J*) in 20 μM FSK exposed BeWo cells. (*K*) Representative images of 20 μM FSK-induced syncytialization of BeWo cells, with the white arrows indicating multinucleated cells. (Scale bar, 40 μm.) (*L*) Quantification of multinucleated cell in *K*. (*M*) Representative FITC-dextran uptake images, measuring macropinocytosis in FSK exposed BeWo cells. (Scale bar, 40 μm.) (*N*) Quantification of FITC intensity. The data are shown as mean ± SD, and analysis was carried out by two-tailed *t* test based at least three independent experiments. $*P < 0.05$; $**P < 0.01$.

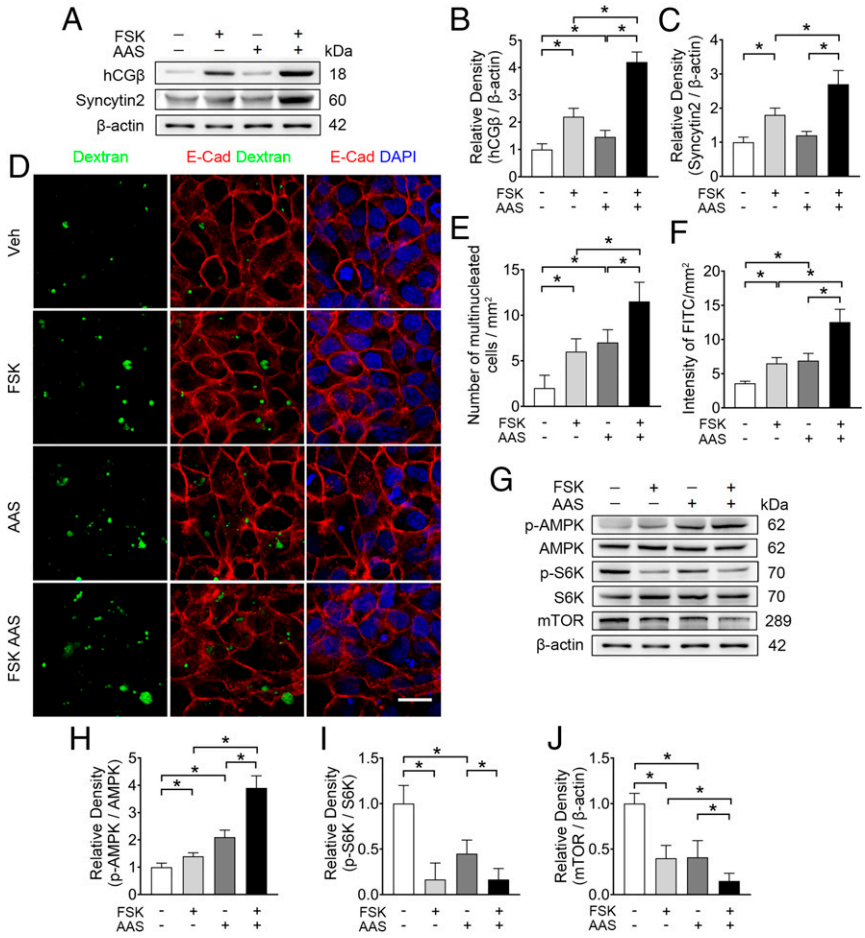

Fig. 2. AAS simultaneously promotes syncytialization and macropinocytosis in BeWo cells. (*A–C*) Western blots (*A*) and corresponding quantification (*B* and *C*) of hCGβ and syncytin2 in BeWo cells cultured in AAS, with concentrations of Lys, Glu, and Arg at one-eighth of the normal levels with or without 20 μM FSK. (*D*) Representative immunostaining of dextran (green), E-cadherin (red), and DAPI (blue) in BeWo cells cultured in conditions detailed. (Scale bar, 40 μm.) (*E* and *F*) Quantification of multinucleated cell and FITC intensity. (*G–J*) Western blots (*G*) and corresponding quantification (*H–J*) of p-AMPK, AMPK, p-S6K, S6K, and mTOR in BeWo cells cultured in the AAS condition with or without 20 μM FSK. (*H–J*) Semiquantification of the relative density of p-AMPK/AMPK, p-S6K/S6K, and mTOR. Data were shown as mean ± SD and analyzed by one-way ANOVA test and Tukey–Kramer multiple comparison test based on at least three independent experiments. $*P < 0.05$.

the effect of AAS medium on syncytium formation and dextran uptake (*SI Appendix*, Fig. S4). Thus, attenuation of mTOR signaling stimulates syncytialization and macropinocytosis in human trophoblast cells.

To further confirm whether mTOR inhibition is necessary for AAS-induced effects, we activated mTOR signaling using MHY1485 in AAS-exposed BeWo cells. We showed that the optimal concentration of MHY1485 that activates mTOR in BeWo cells was 10 μM, as indicated by the p-mTOR/mTOR and p-S6K/S6K (*SI Appendix*, Fig. S5). The joint effects of FSK and AAS on STB marker (hCGβ and Syncytin2) expression, formation of multinucleated morphology, and the macropinocytosis index were abrogated by MHY1485 in BeWo cells (Fig. 3 *H–M*). Together, these data indicate mTOR inhibition is necessary and sufficient for sensing low amino acid supply and for stimulating syncytialization and macropinocytosis in trophoblasts.

mTOR Inhibition in Pregnant Mice Led to Greater Trophoblast Syncytialization and Enhanced Macropinocytosis. To elucidate the significance of trophoblastic macropinocytosis in vivo, pregnant mice were subjected to daily intraperitoneal injection with 1 mg/kg Rapa or vehicle from embryonic day (E)10.5 to E13.5, and fetal and placental outcomes were examined at E14 (Fig. 4*A*). Western blot showed reduced levels of p-mTOR/mTOR and p-S6k/S6k in the placenta upon Rapa administration, confirming a successful blockage of mTOR signaling in vivo (Fig. 4 *B–D*).

In the Rapa-treated dams, fetal weight (FW) (Fig. 4*E*) and placental weight (PW) (Fig. 4*F*) were consistently lower, while the FW/PW ratio was higher than the vehicle controls, suggesting increased placental nutrient transport efficiency upon mTOR inhibition (Fig. 4*G*). To confirm whether trophoblast syncytialization is affected by Rapa treatment, we performed real-time qPCR and found that placental expression of syncytial markers, Gcm1, Syncytin a (Syna), and Syncytin b (Synb) was elevated by at least 50% in Rapa-treated mice (Fig. 4 *H–J*). These data suggest enhanced syncytialization upon Rapa treatment in pregnant mice, consistent with our results in cultured human trophoblasts.

In the mouse placenta, two tightly adjacent layers of STBs (Syn I and Syn II) form a feto–maternal barrier in the labyrinth layer (Fig. 4*K*). Immunofluorescence for monocarboxylate transporter 1 (MCT1; marker for Syn I) and MCT4 (marker for Syn II) demonstrated a clearly transformed alignment of the STB bilayer in Rapa-treated individuals, shown by the expanded separation between the $MCT1^+$ and $MCT4^+$ layers (Fig. 4*L*). Transmission electron microscopy (TEM) of the placentas further demonstrated the striking phenotypic changes in Rapa-treated placenta, including

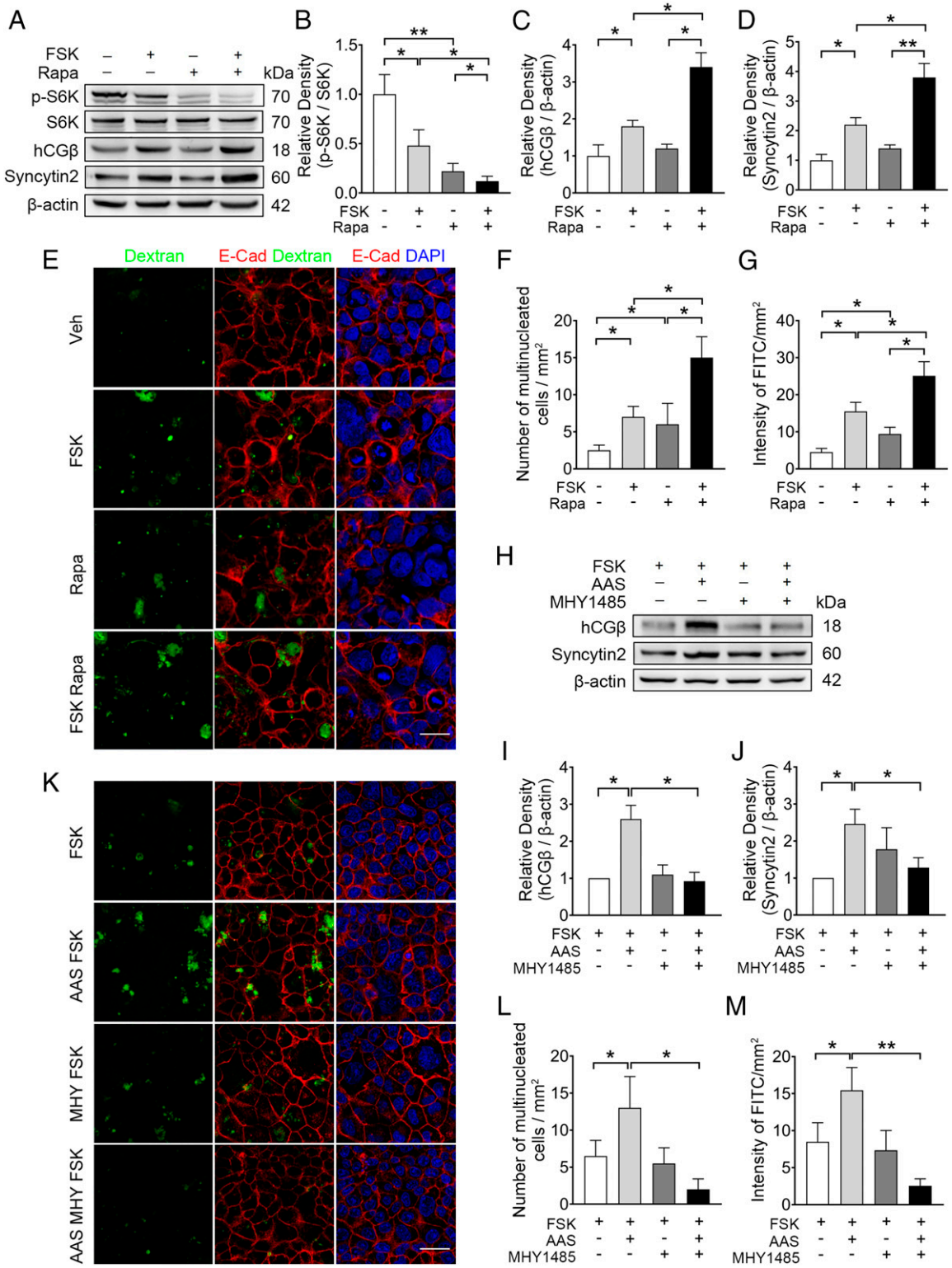

Fig. 3. mTOR inhibition is necessary for the induction of syncytialization and macropinocytosis by FSK in BeWo cells. (*A–D*) Western blots (*A*) and corresponding semiquantification (*B–D*) of p-S6K, S6K, hCGβ,and Syncytin2 in BeWo cells exposed to 100 nM Rapa, with or without 20 μM FSK. (*B–D*) Semiquantification of p-S6K/S6K, hCGβ, and Syncytin2. (*E* and *F*) Representative immunostaining of E-cadherin (red) and DAPI (blue) in BeWo cells cultured in the indicated conditions in *E*. (Scale bar, 40 μm.) (*F*) Quantification of multinucleated BeWo cell. (*E* and *G*) Representative FITC-dextran (green) uptake in BeWo cells, cultured as detailed in *E*. (*G*) Quantification of FITC intensity. (*H–J*) Western blots (*H*) and corresponding quantification (*I* and *J*) of hCGβ and syncytin2 in BeWo cells cultured in AAS media, exposed to 20 μM FSK, with or without 10 μM MHY1485. (*K* and *L*) Representative immunostaining of E-cadherin (red) and DAPI (blue) in BeWo cells cultured as detailed in *K*. (Scale bar, 40 μm.) (*L*) Quantification of multinucleated BeWo cell. (*K* and *M*) Representative FITC-dextran (green) uptake experiment in BeWo cells cultured in indicated conditions in *K*. (*M*) Quantification of FITC intensity. The data are shown as mean ± SD and analyzed by one-way ANOVA test and Tukey–Kramer multiple comparison test based on at least three independent experiments. $*P < 0.05$; $**P < 0.01$.

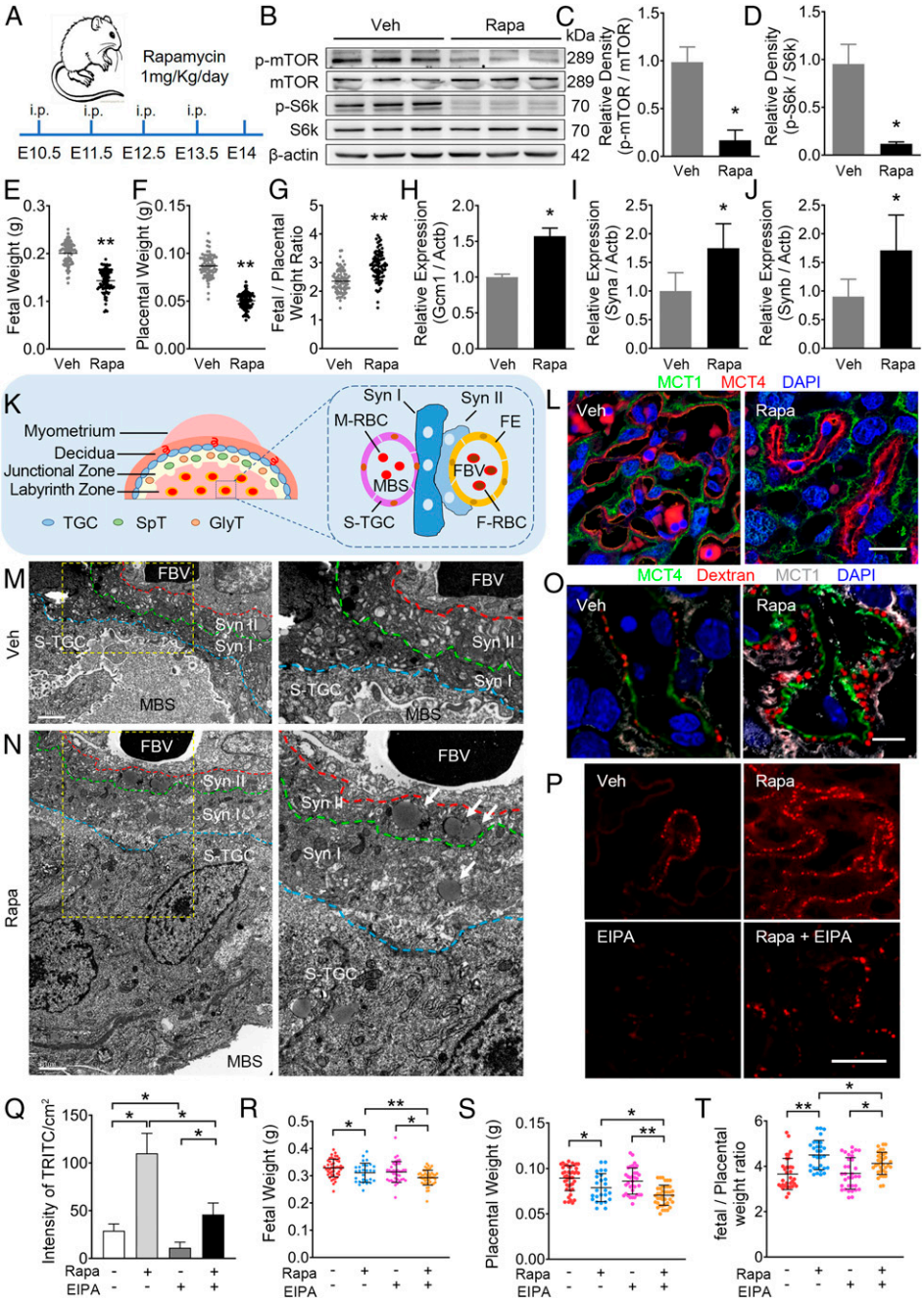

Fig. 4. Inhibition of mTOR signaling by Rapa in pregnant mice leads to enhanced trophoblast syncytialization and macropinocytosis. (*A*) A schematic depiction of the experimental settings. Pregnant CD-1 mice were intraperitoneally injected with 1 mg/kg Rapa or vehicle (DMSO) daily from E10.5 to E13.5, and the mice were killed at E14. (*B–D*) Western blots (*B*) and the corresponding quantification (*C* and *D*) of p-mTOR, mTOR, p-S6k, and S6k in mouse placentas treated with vehicle ($n = 10$) or Rapa ($n = 10$). (*C* and *D*) Semiquantification of p-mTOR/mTOR and p-S6k/S6k. (*E–G*) FW (*E*), PW (*F*), and FW/PW weight ratio (*G*) in vehicle or Rapa dams. (*H–J*) mRNA levels of STB makers, Gcm1 (*H*), Syna (*I*), and Synb (*J*), in placentas from mice treated with vehicle or Rapa. (*K*) Schematic depiction of the mouse placenta. FE, fetal endothelium; FBV, fetal blood vessel; F-RBC, fetal red blood cell; GlyT, glycogen trophoblast; MBS, maternal blood sinus; M-RBC, maternal red blood cell; SpT, spongiotrophoblast; S-TGC, sinusoidal trophoblast giant cell; Syn I, the first layer of STB; Syn II, the second layer of STB; TGC, trophoblast giant cell. (*L*) Immunofluorescent staining of MCT1 (green), MCT4 (red) in the indicated placentas. Scale bar, 20 μm. (*M* and *N*) Representative TEM images of STBs in mouse placentas treated with vehicle (*M*, $n = 6$) or Rapa (*N*, $n = 6$). *Right* in *M* and *N* are the corresponding higher magnification images of the yellow frame *Insets* (*Left*). White arrows, large vesicles (0.2 to ∼5 μm in diameter, indicating macropinosomes) observed in Syn II of Rapa-treated mice. (Scale bars, 1 μm; magnification used in enlargements, 2×) (*O*) Three mice per group were subjected to single-injection of 2 mg/kg TRITC-dextran (intravenously) 3 min before being killed. Representative confocal images of TRITC-dextran (red) uptake in mouse STBs illustrated by MCT4 (green) or MCT1 (white) in vehicle or Rapa. (Scale bar, 20 μm.) (*P–T*) Pregnant CD-1 mice were injected from E10.5 to E13.5 with vehicle (DMSO, intraperitoneally and/or intravenously, $n = 5$), 1 mg/kg/d of Rapa (intraperitoneally, $n = 5$), 1 mg/kg/d of EIPA (intravenously, $n = 5$), and combination of Rapa and EIPA ($n = 5$), respectively. The placenta tissues were collected at E14. (*P*) Representative staining of TRITC-dextran (red) in the indicated E14 placentas of vehicle (DMSO, $n = 3$), Rapa- ($n = 3$), EIPA- ($n = 3$), and Rapa+EIPA- ($n = 3$) treated mice. (Scale bar, 40 μm.) (*Q*) Quantification of TRITC intensity in the indicated mouse placentas. (*R–T*) FW (*R*), PW (*S*), and FW/PW weight ratio (*T*) in vehicle-, Rapa-, EIPA-, and Rapa+EIPA-treated groups. The data are shown as mean ± SD, and the analysis was carried out by two-tailed *t* test (*C–J*) or one-way ANOVA test and Tukey–Kramer multiple-comparison test (*Q–S*). $*P < 0.05$; $**P < 0.01$.

thickened syncytial layers, and increased distance between fetal blood vessel and maternal blood sinus (Fig. 4 *M* and *N*).

To measure macropinocytosis in the mouse placenta, TRITC-dextran (>70 kDa) was injected intravenously 3 min prior to killing. Immunofluorescent analysis showed dim TRITC-dextran puncta in STB of vehicle placentas (Fig. 4*O*). In contrast, Rapa-treated placentas displayed strong dextran signal in STB layers (Fig. 4*O*). Consistently, TEM revealed a massive accumulation of large vesicles, an indicator of macropinosomes, in the STB of Rapa-exposed placentas (Fig. 4*N*, white arrows). These placental phenotypes indicate the enhanced macropinocytosis in the syncytium upon Rapa treatment in mice.

Blockage of Macropinocytosis in Pregnant Mice Worsened FGR. To assess the physiological significance of macropinocytosis during pregnancy, both Rapa- and vehicle-treated mice were injected daily (E10.5 to E13.5) intravenously with 5-(*N*-ethyl-*N*-isopropyl) amiloride (EIPA), a specific inhibitor of macropinocytosis (14), and outcomes were determined at E14.0. As shown in Fig. 4 *P* and *Q*, TRITC-dextran uptake was significantly weakened by EIPA administration in both vehicle and Rapa mice. Intriguingly, the Rapa+EIPA mice exhibited a further decrease in both FW and PW compared with Rapa mice, and the ratio of FW/PW was 15% lower than that of the Rapa group (Fig. 4 *R*–*T*). These results suggest that blockage of macropinocytosis in the placenta diminishes the macropinocytosis-dependent placental transport, leading to an adverse impact on fetal growth.

Repressed mTOR Signaling and Increased Trophoblast Syncytialization in Human FGR Placenta. To further evaluate the pathological relevance of macropinocytosis in FGR patients, we assessed mTOR activity and syncytialization in human FGR-related and normal control placentas. The levels of p-S6K/S6K and p-mTOR/mTOR in FGR placentas were around 60% of controls (Fig. 5 *A*–*C*), confirming that mTOR signaling is repressed in FGR-related placentas, and suggesting an insufficient nutrient supply to the FGR placenta. Measurement of the syncytialization of FGR placentas showed the elevated levels of hCGβ and Syncytin2 by 51% and 26%, respectively (Fig. 5 *A*, *D*, and *E*), and the average nuclear number in syncytium was 1.6-fold higher than the controls (Fig. 5 *F* and *G*). These data are consistent with previous reports that maternal serum hCG was higher in FGR patients, and syncytial nuclei accumulated at the villous surface in FGR placentas (23–25). Accordingly, mTOR activity, determined by p-S6K/S6K or p-mTOR/mTOR, negatively correlated with hCGβ and Syncytin2 expression in FGR placenta (*SI Appendix*, Fig. S6 *A*–*D*). These findings suggest a link between excessive trophoblast syncytialization and repressed mTOR signaling in human FGR placenta.

Considering the gestational age difference between the FGR and control placentas is about 4 to 5 wk (as shown in *SI Appendix*, Table S1), we collected 10 placentas from women with unexplained preterm labor (PTL), matched with the FGR placentas based on the gestational age at birth. The levels of p-S6K/S6K, p-mTOR/mTOR, mTOR, hCGβ, and Syncytin2 in the PTL placentas were comparable to the control placentas (*SI Appendix*, Fig. S6 *E*–*J*), suggesting that the difference in syncytialization and mTOR signaling observed in the FGR placentas is unlikely due to different gestational age at delivery, but reflects intrinsic changes in the FGR placenta.

We subjected PHT cells from FGR and control placentas to spontaneous cell fusion, and found that the FGR-derived PHT cells exhibited significantly increased *hCGB* and Syncytin2 levels during the syncytialization process compared to the corresponding control cells (Fig. 5 *H*–*J*). Again, PHT cells from PTL placentas showed a similar pattern of *hCGB* as the control cells (*SI Appendix*, Fig. S6*K*). These data further prove that trophoblasts from FGR placenta exhibited increased ability to syncytialize. As expected, the extent of FITC-dextran uptake in FGR-PHT cells was significantly higher (1.8-fold at 72 h) than the controls (Fig. 5 *K* and *L*). In addition, TEM observation revealed the accumulation of large vesicles, pointing to a greater abundance of macropinosomes in FGR placental STB (Fig. 5 *M* and *N*, white arrows). These observations demonstrate the enhanced macropinocytosis in human FGR placenta, which is in line with the enhanced trophoblast differentiation in these placentas.

Discussion

Mammalian pregnancy involves nutritional allocation between the mother and the fetus, which critically impacts fetal growth and pregnancy viability, in particular when nutrients are scarce. Disrupted nutrient homeostasis may lead to compromised fetal–maternal health (26), thus creating a selective pressure to adapt to diminished resources. The placenta constitutes the main interface between the mother and fetus and is believed to shape mammalian pregnancy outcomes by sophisticatedly adapting to the nutrient environment. Almost all nutrients transferred to the fetus must be either actively or passively transported across the polarized plasma membrane of the placental STB, a highly specialized multinucleated epithelial cell layer covering the surface of the chorionic villi (27). The trophoblast cells possess various transporters for glucose, amino acids, and fatty acid and are believed to preferentially utilize these low molecular-weight nutrients. However, maternal exposure to nutrient insufficiency or hypoxia, hypoperfusion, or impaired maternal cardiovascular function, will cause restricted nutrient supply to the placenta. Therefore, the rapid and appropriate adaptation to nutrient fluctuation in the placenta is critical to guarantee fetal survival and growth under nutrient deprivation. The work presented here intensively reveals the structural and functional plasticity of the placental syncytium, which adapts to nutrient scarcity by macropinocytosis as an alternative nutrient source to allow sustained fetal growth. The tight association between enhanced syncytialization and macropinocytosis, and accumulation of large macropinosome vesicles in syncytium in the FGR placenta represent an adaptive response to safeguard fetal growth needs, akin to podocytes and tumor cells where macropinocytosis facilitates direct nutrient supply, specifically through degrading the scavenged proteins into amino acids (7, 13, 14). Our data thus underscore the physiological significance of trophoblast syncytialization as a part of pregnancy adaptation to a nutrient-deficient environment (Fig. 6).

The cellular uptake of amino acids via transporters or macropinocytosis under the control of mTOR activity is of great physiological significance. Proteins are the most abundant organic constituents in body fluids, whereas mammalian cells preferentially metabolize low molecular-weight nutrients, such as glucose and amino acids (14, 28). Amino acid sufficiency represents an essential input for mTORC1 activation in mammalian cells (28). During limited periods of nutrient deprivation, inactivation of mTORC1 triggers the formation of autophagosomes to engulf intracellular constituents, and the autophagic degradation of intracellular proteins provides recycling amino acids for adaptive protein synthesis to sustain cell survival (29). While upon persistent nutrient deprivation, suppression of mTORC1 and activation of Ras signal enable cells to utilize pinocytotic extracellular proteins as a source of amino acids and meet the increase in biomass of sustained cell viability. Amino acids induced mTORC1 recruitment to lysosomal membranes, and the subsequent mTORC1 activation by growth factor signaling (29) allows lysosomal mTORC1 to monitor amino acids recovered from proteins that were delivered through endocytosis or autophagy. Within the unique microenvironment of placental STBs, where nutrient supply utterly depends on maternal blood perfusion to the intervillous space, sensing of nutrient status in placental syncytium by mTOR activity may efficiently orchestrate

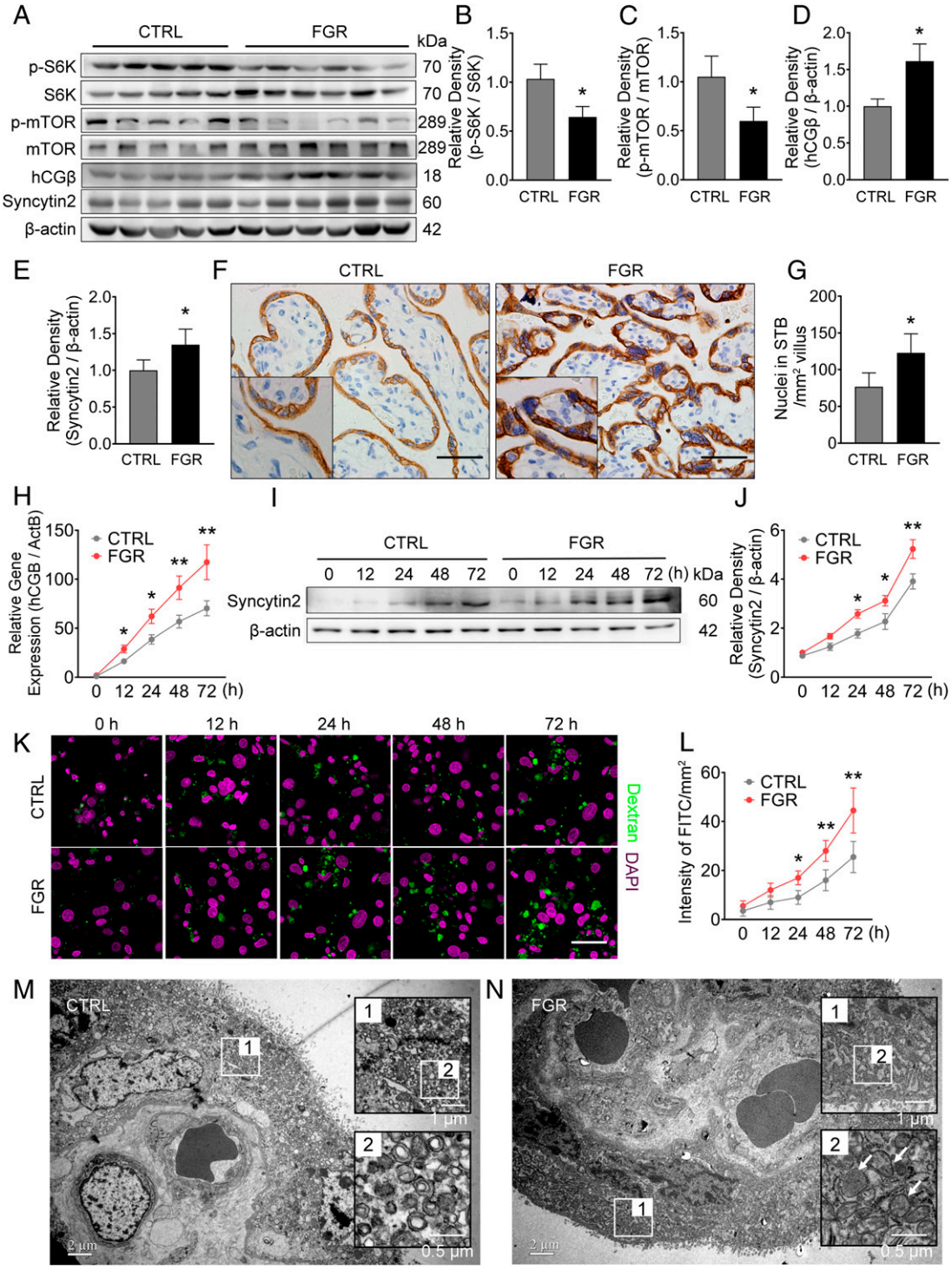

Fig. 5. Syncytialization, macropinocytosis activity, and mTOR signaling in normal or FGR human placentas. Sixteen control and 14 FGR placentas were collected and analyzed. (*A–E*) Western Blots (*A*) and corresponding quantification (*B–E*) of p-S6K, S6K, p-mTOR, mTOR, hCGβ, and Syncytin2 in control and FGR placentas. (*F* and *G*) Quantification of the number of nuclei in STB of control and FGR placentas based on the immunohistochemistry staining of Cytokeratin 7 (*F*, higher magnification of images are displayed as *Insets*). (*G*) Quantification of nuclear number in STB. Three placentas from each group were included, and three slides per sample were subjected to immunohistochemistry. The number of nuclei in the STB was counted in five random fields of each slide and presented as nuclear number per square millimeter of villous area. The results are presented as mean ± SD, and statistically analyzed by two-tailed *t* test. (Scale bars, 400 μm; magnification used in enlargements in *F*, 2×) (*H–J*) mRNA level of *hCGB* (*H*) and Western blot of syncytin2 (*I* and *J*) in primary cultured trophoblasts derived from control or FGR placentas. (*K*) Representative images of FITC-dextran uptake indicating macropinocytosis in PHT cells derived from control or FGR placenta, with green and magenta signal indicating FITC-dextran and DAPI, respectively. (Scale bar, 20 μm.) (*L*) Quantification of FITC intensity. (*M* and *N*) Representative TEM images of STBs from normal pregnancy (*M*, $n = 5$) vs. FGR (*N*, $n = 5$) placentas. The panel in black frames are regional magnification of the corresponding white frames, with white arrows indicating large vesicles (0.2 to ∼5 μm in diameter, indicating macropinosomes) observed in the STBs of the FGR placenta. The data are shown as mean ± SD, analyzed by two-tailed *t* test based on the results from at least three independent experiments. $*P < 0.05$; $**P < 0.01$.

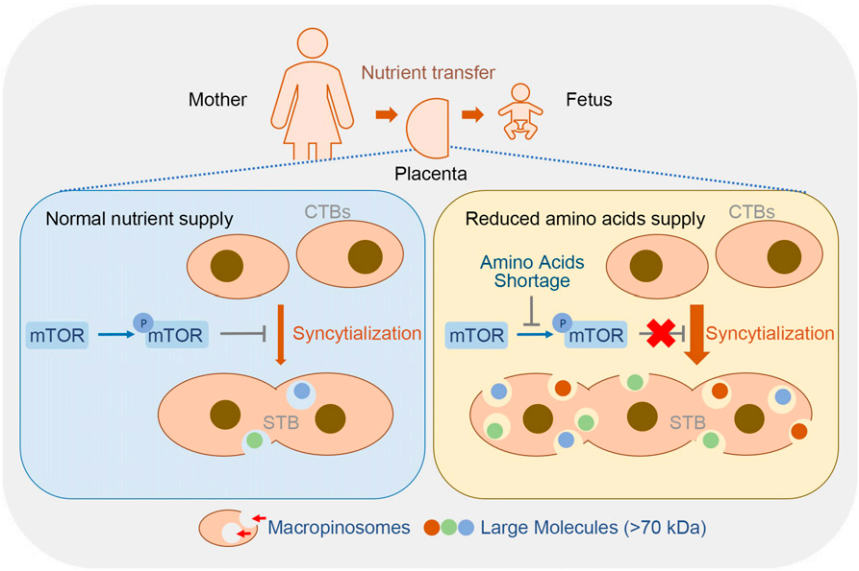

Fig. 6. A model of macropinocytosis-mediated adaptation to nutritional stress in STB. Macropinocytosis in trophoblasts positively correlates with syncytialization. The syncytialized placental trophoblasts can efficiently uptake large molecules (>70 kDa) by the macropinocytosis machinery, which is enhanced during reduced amino acid supply. AAS induces trophoblast syncytialization and activates macropinocytosis by inhibiting mTOR phosphorylation and activation.

transporter-mediated amino acid uptake or extracellular protein macropinocytosis. This mechanism presents a flexible strategy that enables the placenta to efficiently adapt to nutrient fluctuation and stably provide biosynthetic substrates to the growing fetus. And indeed, there has been evidence demonstrating the requirement of placental mTOR activation in promoting the plasma membrane expression of specific system A (SNAT2, SLC38A2) and system L (LAT1, SLC7A5) transporter isoforms (30, 31). The activities of placental transporters for amino acids are remarkably reduced in FGR (32), where mTOR activity is evidently repressed.

The links among mTOR signaling, syncytialization, and macropinocytosis in the placenta have been undefined. We found that exposure of BeWo cells to AAS or rapamycin activated the PKA signal (*SI Appendix*, Fig. S7 *A–D*). Cyclic AMP-dependent PKA signaling is known to essentially trigger trophoblast syncytialization (6). It is therefore likely that mTOR inhibition enhances trophoblast syncytialization through activation of the PKA signal. Studies in other cell types demonstrated the induction of autophagy by mTORC1 repression (29, 33), and the induction of autophagy activated the PKA signal (34). Interestingly, we observed enhanced autophagy in BeWo cells upon exposure to AAS or rapamycin (*SI Appendix*, Fig. S7 *E–J*). In addition, studies in cancer cells have demonstrated that Ras activation directs macropinocytosis of extracellular protein and reduces cell dependence on exogenous amino acid supply (13, 35), and mTORC1 inhibition specifically enhanced the protein degradation in lysosomes (14). A proteomic profiling of FSK-induced trophoblasts revealed a significant increase in phosphorylated Ras in syncytialized trophoblast (36). We therefore propose that trophoblastic mTORC1 signal is repressed by sensing amino acid-insufficient conditions, which subsequently activates cAMP-PKA signaling, likely through enhanced autophagy, and further stimulates Ras signaling. Thus, trophoblast syncytialization is coupled with macropinocytosis.

Amino acid abundance may not the sole upstream regulator of mTOR activity. Nutrients such as glucose may also regulate mTOR signaling through ATP production, as low ATP levels activate AMPK and subsequently lead to mTOR inactivation (37). Besides, mTORC1 has a multitude of upstream regulators, including hormones and growth factors such as insulin, IGF-I, EGF, hypoxia, and fatty acids (33). Growth factor-dependent activation of mTORC1 by amino acids, but not glucose, requires macropinocytosis (38). Therefore, further studies are needed to clarify which hormones or growth factors couple nutrient signals to mTORC1 and macropinocytosis in syncytialized trophoblasts. Meanwhile, it remains to be elucidated whether trophoblastic macropinocytosis is principally regulated by mTORC1 rather than mTORC2, as reported by Palm et al. (14) in K-Ras^{G12D} mouse embryonic fibroblasts.

An interesting question to be addressed is whether gestational stage-dependent mechanisms regulate macropinocytosis in trophoblasts. It has been reported that once the trophoblast cell fusion process gets started, the differentiation process and regulatory mechanism are roughly similar throughout gestation (6, 39). However, single-cell maps revealed varied placental cell subtypes and properties at different pregnant stages, along with the change in fetal demanding (40, 41). An elaborate comparison of the regulation in nutrient absorption and metabolism in placental trophoblasts at different gestational stages is worthy of further exploration.

One limitation of this study is that in vivo assays in pregnant mice largely rely on the use of pharmacological inhibitors and activators rather than genetic approaches. A big obstacle is that deficiency in *mtor* or *raptor* leads to early fetal lethality in mice (E6.5 to E7.5) (42, 43). We thus treated the pregnant mice with a low dosage of rapamycin for a short period in order to mimic maternal mal- or undernutrition. The inhibition of macropinocytosis using gene-targeting approaches has been hampered by a lack of signature molecules for such a process (7, 44). EIPA is a commonly used macropinocytosis inhibitor (13, 14, 45), which we utilized in pregnant mice at a relatively low dose in order to avoid influencing maternal health and fetal growth (as shown in Fig. 4 *R–T*).

Another limitation of this study is that we have not pursued the fate of scavenged large molecules in STB. One possibility is that these molecules may be transported to lysosomes for degradation and utilized as an energy source, or as recycled building blocks for cellular components, as has been reported in podocytes and tumor cells (7, 13). Our observations that a shortage of amino acids (Arg, Lys, and Glu) enhances macropinocytosis in

syncytialized trophoblasts, and inhibition of macropinocytosis with EIPA reduces feto-placental weight support the notion that large macropinocytosed molecules in STB may be utilized as a nutrient source to the growing fetus.

In total, our study highlights an important compensatory pathway for placental multinucleated trophoblasts to up-regulate nutrient delivery in the context of limiting maternal nutrient supply. Our findings may stimulate the development of therapeutic approaches to support the fetus during maternal malnutrition or other conditions that jeopardize placental nutrient transport.

Materials and Methods

Study Participants and Samples. The Ethics Committee of the Institute of Zoology, Chinese Academy of Sciences, and Guangzhou Medical University Third Hospital approved the study protocol for the collection of human placenta tissues. A written consent was obtained from all pregnant women enrolled in the study.

Placenta samples were collected from 40 nulliparous pregnant women who underwent regular prenatal care at Guangzhou Medical University Third Hospital from June 2016 to December 2017. The placentas were collected within 1 h of Caesarean sections, and biopsies of the basal plate were separately collected from the placenta disk at sites located 5 cm from the umbilical cord insertion site. These biopsies were snap-frozen in liquid nitrogen or fixed for TEM. Full-thickness specimens encompassing the chorionic and basal plate were subjected to routine paraffin embedding and sectioning. Additional details on the determination of pregnancy outcome and the clinical characteristics of the enrolled patients are summarized in *SI Appendix, Supplementary Experimental Procedures* and Table S1.

Culture of PHT Cells from Human Term Placenta and Trophoblast Cell Line. Isolation of CTB from the human placenta was performed as described previously (46). Human choriocarcinoma cell line BeWo and JEG-3 cells, and hepatocellular carcinoma cell line HepG2 cells were purchased from the American Type Culture Collection. Additional details on CTB isolation and cell culture procedure are available in *SI Appendix*.

For AAS experiments, the cells were maintained in medium of a 7:1 mixture of DMEM depleted of amino acids glutamine, lysine, and arginine (Gibco A14431-01) and regular high-glucose DMEM (Gibco 11965-092), supplemented with 10% FBS and sodium pyruvate.

Western Blot Analysis, RNA Extraction, and Reverse-Transcription Quantitative PCR (RT-qPCR) and Immunohistochemistry. Western blot, RNA extraction, RT-qPCR, and immunohistochemistry were performed using standard procedures. Additional details are available in *SI Appendix*.

Knockdown Using Specific siRNA. BeWo cells were seeded onto 24-well plates at 20,000 cells per well and transiently transfected using Lipofectamine 2000 (Thermo Scientific) with 100 nM of specific siRNA targeting human raptor (sc-44069; Santa Cruz Biotechnology), or nonspecific scramble siRNAs (GenePharma) as negative controls. Following 4 h of transfection, the media were replaced with fresh F-12K:DMEM media supplemented with 10% FBS and sodium pyruvate. The cells were harvested for further analysis at 48 h posttransfection.

Immunofluorescence Staining and Confocal Microscopy. Freshly collected placental tissues were fixed in 4% paraformaldehyde (Sigma Aldrich) at 4 to 8 °C and embedded in Tissue-Tek OCT compound (Sakura Finetek). Frozen sections of 8-μm thickness was incubated with antibodies against MCT1 or MCT4 (*SI Appendix*, Table S2), followed by a FITC-conjugated or TRITC-conjugated secondary antibody (Zhongshan Golden Bridge), and the cell nuclei were stained with DAPI (Sigma Aldrich). The results were analyzed using a laser confocal microscope (Leica).

Mouse Model and Treatments In Vivo. All experiments using mice were approved by the Institutional Animal Care and Use Committee of Institute of Zoology, Chinese Academy of Sciences. Virgin CD-1 female mice (8- to 12-wk old) were mated with fertile males (10-wk old), and the day on which the vaginal plug was detected was recorded as E0.5. The pregnant mice were randomly divided into four treatment groups with at least 10 animals per group: Vehicle (DMSO), Rapa, EIPA, Rapa+EIPA, in which the dams were injected from E10.5 to E13.5 with vehicle (DMSO, intraperitoneally), 1 mg/kg/d of Rapa (intraperitoneally), 1 mg/kg/d of EIPA (intravenously), or a combination of Rapa and EIPA. The mice were killed at E14, and the placental tissues were collected. In order to imaging macropinocytosis in the placenta, three mice per group were subjected to single injection of 2 mg/kg TRITC-dextran (intravenously) 3 min before being killed.

TEM. In total, five pairs of FGR and control human placentas were enrolled for the TEM experiment. For each placenta, biopsies of the fresh tissues (0.5 cm^3) were collected from three different sites located 5 cm from the umbilical cord insertion site. The mouse placental tissues at 0.2 cm^3 were freshly collected in triplicate across the umbilical cord insertion. In total, six placentas from each group (treatment with Rapa or DMSO) were included for TEM. The collected tissues were quickly immersed in 2.5% glutaraldehyde and 2% paraformaldehyde in sodium cacodylate buffer, followed by fixation with 1% osmic acid. After routine dehydration, the tissues were embedded in epoxy resin. Ultrathin sections were mounted on 200-mesh grids and stained with uranyl acetate and lead citrate. The results were observed using a JEM-1400 TEM (JEOL).

Statistical Analysis. All statistical analyses were performed with SPSS 18.0 software package (IBM). The nonparametric Spearman correlation test was used to analyze the correlation of p-S6K/S6K, p-mTOR/mTOR, hCGβ, and Syncytin2. Data of qPCR and Western blotting were reported as mean ± SD, based on at least three independent experiments. Differences between groups were analyzed using independent sample *t* test or one-way ANOVA (for normally distributed data), followed by post hoc Turkey–Kramer multiple comparison analysis. The differences were considered significance at $P < 0.05$.

Data Availability. All study data are included in the article and supporting information.

ACKNOWLEDGMENTS. We thank Dr. Nicolas Plachta at Institute of Molecular & Cell Biology, Agency for Science, Technology & Research (A*STAR), Singapore for the critical comments and help in revising the manuscript; and Drs. Hongmei Wang and Ruoxuan Yu for technical assistance in isolating trophoblasts from term placenta. The study was supported by National Key Research and Development Program of China Grants 2018YFC1004100 and 2016YFC1000200 (to Y.-L.W.), 2018YFC1004400 (to B.C.), and 2016YFC1000401 and 2017YFC1001404 (to M.L.); National Natural Science Foundation in China Grants 81730040 (to Y.-L.W.), 81971414 (to B.C.), and 31800986 (to X.S.); and Natural Science Foundation of Fujian Province of China Grant 2020J06003 (to B.C.).

1. S. A. Anin, G. Vince, S. Quenby, Trophoblast invasion. *Hum. Fertil. (Camb.)* **7**, 169–174 (2004).
2. G. Lin *et al*., Improving amino acid nutrition to prevent intrauterine growth restriction in mammals. *Amino Acids* **46**, 1605–1623 (2014).
3. S. Zhang *et al*., Placental adaptations in growth restriction. *Nutrients* **7**, 360–389 (2015).
4. G. Mandruzzato *et al*.; WAPM, Intrauterine restriction (IUGR). *J. Perinat. Med.* **36**, 277–281 (2008).
5. D. D. McIntire, S. L. Bloom, B. M. Casey, K. J. Leveno, Birth weight in relation to morbidity and mortality among newborn infants. *N. Engl. J. Med.* **340**, 1234–1238 (1999).
6. L. Ji *et al*., Placental trophoblast cell differentiation: Physiological regulation and pathological relevance to preeclampsia. *Mol. Aspects Med.* **34**, 981–1023 (2013).
7. J. J. Chung *et al*., Albumin-associated free fatty acids induce macropinocytosis in podocytes. *J. Clin. Invest.* **125**, 2307–2316 (2015).
8. G. J. Doherty, H. T. McMahon, Mechanisms of endocytosis. *Annu. Rev. Biochem.* **78**, 857–902 (2009).
9. C. C. Norbury, L. J. Hewlett, A. R. Prescott, N. Shastri, C. Watts, Class I MHC presentation of exogenous soluble antigen via macropinocytosis in bone marrow macrophages. *Immunity* **3**, 783–791 (1995).
10. F. Sallusto, M. Cella, C. Danieli, A. Lanzavecchia, Dendritic cells use macropinocytosis and the mannose receptor to concentrate macromolecules in the major histocompatibility complex class II compartment: Downregulation by cytokines and bacterial products. *J. Exp. Med.* **182**, 389–400 (1995).
11. M. C. Kerr, R. D. Teasdale, Defining macropinocytosis. *Traffic* **10**, 364–371 (2009).
12. S. Watanabe, E. Boucrot, Fast and ultrafast endocytosis. *Curr. Opin. Cell Biol.* **47**, 64–71 (2017).
13. C. Commisso *et al*., Macropinocytosis of protein is an amino acid supply route in Ras-transformed cells. *Nature* **497**, 633–637 (2013).
14. W. Palm *et al*., The utilization of extracellular proteins as nutrients is suppressed by mTORC1. *Cell* **162**, 259–270 (2015).
15. Y. Li *et al*., Involvement of nephrin in human placental trophoblast syncytialization. *Reproduction* **149**, 339–346 (2015).
16. T. L. Thirkill, G. C. Douglas, Differentiation of human trophoblast cells in vitro is inhibited by dimethylsulfoxide. *J. Cell. Biochem.* **65**, 460–468 (1997).

17. S. Al-Nasiry, B. Spitz, M. Hanssens, C. Luyten, R. Pijnenborg, Differential effects of inducers of syncytialization and apoptosis on BeWo and JEG-3 choriocarcinoma cells. *Hum. Reprod.* **21**, 193–201 (2006).
18. M. Nofal, K. Zhang, S. Han, J. D. Rabinowitz, mTOR inhibition restores amino acid balance in cells dependent on catabolism of extracellular protein. *Mol. Cell* **67**, 936–946.e5 (2017).
19. C. T. Cheng *et al*., Arginine starvation kills tumor cells through aspartate exhaustion and mitochondrial dysfunction. *Commun. Biol.* **1**, 178 (2018).
20. J. Joutsen *et al*., Heat shock factor 2 protects against proteotoxicity by maintaining cell-cell adhesion. *Cell Rep.* **30**, 583–597.e6 (2020).
21. S. C. Lin, D. G. Hardie, AMPK: Sensing glucose as well as cellular energy status. *Cell Metab.* **27**, 299–313 (2018).
22. S. Wullschleger, R. Loewith, M. N. Hall, TOR signaling in growth and metabolism. *Cell* **124**, 471–484 (2006).
23. J. L. Bartha, R. Comino-Delgado, J. Arrabal, M. A. Escobar, Third-trimester maternal serum beta-HCG level and umbilical blood flow in fetal growth retardation. *Int. J. Gynaecol. Obstet.* **57**, 27–31 (1997).
24. I. P. Crocker, D. M. Tansinda, P. N. Baker, Altered cell kinetics in cultured placental villous explants in pregnancies complicated by pre-eclampsia and intrauterine growth restriction. *J. Pathol.* **204**, 11–18 (2004).
25. R. Gonen *et al*., The association between unexplained second-trimester maternal serum hCG elevation and pregnancy complications. *Obstet. Gynecol.* **80**, 83–86 (1992).
26. P. Díaz, T. L. Powell, T. Jansson, The role of placental nutrient sensing in maternal-fetal resource allocation. *Biol. Reprod.* **91**, 82 (2014).
27. K. Red-Horse *et al*., Trophoblast differentiation during embryo implantation and formation of the maternal-fetal interface. *J. Clin. Invest.* **114**, 744–754 (2004).
28. R. Milanesi, P. Coccetti, F. Tripodi, The regulatory role of key metabolites in the control of cell signaling. *Biomolecules* **10**, 862 (2020).
29. Y. Sancak *et al*., Ragulator-Rag complex targets mTORC1 to the lysosomal surface and is necessary for its activation by amino acids. *Cell* **141**, 290–303 (2010).
30. F. J. Rosario, T. L. Powell, T. Jansson, Mechanistic target of rapamycin (mTOR) regulates trophoblast folate uptake by modulating the cell surface expression of FR-α and the RFC. *Sci. Rep.* **6**, 31705 (2016).
31. F. J. Rosario, T. L. Powell, T. Jansson, mTOR folate sensing links folate availability to trophoblast cell function. *J. Physiol.* **595**, 4189–4206 (2017).
32. S. Roos, T. L. Powell, T. Jansson, Placental mTOR links maternal nutrient availability to fetal growth. *Biochem. Soc. Trans.* **37**, 295–298 (2009).
33. R. A. Saxton, D. M. Sabatini, mTOR signaling in growth, metabolism, and disease. *Cell* **168**, 960–976 (2017).
34. S. Hu *et al*., Autophagy induces transforming growth factor-β-dependent epithelial-mesenchymal transition in hepatocarcinoma cells through cAMP response element binding signalling. *J. Cell. Mol. Med.* **22**, 5518–5532 (2018).
35. D. Bar-Sagi, J. R. Feramisco, Induction of membrane ruffling and fluid-phase pinocytosis in quiescent fibroblasts by ras proteins. *Science* **233**, 1061–1068 (1986).
36. L. P. Nampoothiri, P. S. Neelima, A. J. Rao, Proteomic profiling of forskolin-induced differentiated BeWo cells: An in-vitro model of cytotrophoblast differentiation. *Reprod. Biomed. Online* **14**, 477–487 (2007).
37. K. Inoki, T. Zhu, K. L. Guan, TSC2 mediates cellular energy response to control cell growth and survival. *Cell* **115**, 577–590 (2003).
38. S. Yoshida, R. Pacitto, Y. Yao, K. Inoki, J. A. Swanson, Growth factor signaling to mTORC1 by amino acid-laden macropinosomes. *J. Cell Biol.* **211**, 159–172 (2015).
39. B. Huppertz, M. Gauster, Trophoblast fusion. *Adv. Exp. Med. Biol.* **713**, 81–95 (2011).
40. R. Pique-Regi *et al*., Single cell transcriptional signatures of the human placenta in term and preterm parturition. *eLife* **8**, e52004 (2019).
41. R. Vento-Tormo *et al*., Single-cell reconstruction of the early maternal-fetal interface in humans. *Nature* **563**, 347–353 (2018).
42. Y. G. Gangloff *et al*., Disruption of the mouse mTOR gene leads to early post-implantation lethality and prohibits embryonic stem cell development. *Mol. Cell. Biol.* **24**, 9508–9516 (2004).
43. M. Murakami *et al*., mTOR is essential for growth and proliferation in early mouse embryos and embryonic stem cells. *Mol. Cell. Biol.* **24**, 6710–6718 (2004).
44. L. Li *et al*., The effect of the size of fluorescent dextran on its endocytic pathway. *Cell Biol. Int.* **39**, 531–539 (2015).
45. N. Tejeda-Muñoz, L. V. Albrecht, M. H. Bui, E. M. De Robertis, Wnt canonical pathway activates macropinocytosis and lysosomal degradation of extracellular proteins. *Proc. Natl. Acad. Sci. U.S.A.* **116**, 10402–10411 (2019).
46. H. J. Kliman, J. E. Nestler, E. Sermasi, J. M. Sanger, J. F. Strauss 3rd, Purification, characterization, and in vitro differentiation of cytotrophoblasts from human term placentae. *Endocrinology* **118**, 1567–1582 (1986).
47. S. W. Lee *et al*., EGFR-pak signaling selectively regulates glutamine deprivation-induced macropinocytosis. *Dev. Cell* **50**, 381–392.e5 (2019).